Spectroscopic Evidence for a Unique Bonding Interaction in Oxo-Molybdenum Dithiolate Complexes: Implications for σ Electron Transfer Pathways in the Pyranopterin Dithiolate Centers of Enzymes

Frank E. Inscore,[†] Rebecca McNaughton,[†] Barry L. Westcott,[‡] Matthew E. Helton,[†] Robert Jones,[†] Ish K. Dhawan,[‡] John H. Enemark,*[,‡] and Martin L. Kirk*[,†]

Department of Chemistry, The University of New Mexico, Albuquerque, New Mexico 81731-1096, and Department of Chemistry, The University of Arizona, Tucson, Arizona 85721-0041

Received September 18, 1998

Solution and solid state electronic absorption, magnetic circular dichroism, and resonance Raman spectroscopies have been used to probe in detail the excited state electronic structure of LMoO(bdt) and LMoO(tdt) (L = hydrotris-(3,5-dimethyl-1-pyrazolyl)borate; bdt = 1,2-benzenedithiolate; tdt = 3,4-toluenedithiolate). The observed energies, intensities, and MCD band patterns are found to be characteristic of LMoO(S-S) compounds, where (S-S) is a dithiolate ligand which forms a five-membered chelate ring with Mo. Ab initio calculations on the 1,2-ene-dithiolate ligand fragment, $^{-}$SC=CS^{-}, show that the low-energy S → Mo charge transfer transitions result from one-electron promotions originating from an isolated set of four filled dithiolate orbitals that are primarily sulfur in character. Resonance Raman excitation profiles have allowed for the definitive assignment of the ene-dithiolate $S_{in-plane}$ → Mo d_{xy} charge transfer transition. This is a bonding-to-antibonding transition, and its intensity directly probes sulfur covalency contributions to the redox orbital (Mo d_{xy}). Raman spectroscopy has identified three totally symmetric vibrational modes at 362 cm^{-1} (S−Mo−S bend), 393 cm^{-1} (S−Mo−S stretch), and 932 cm^{-1} (Mo≡O stretch), in contrast to the large number low-frequency modes observed in the resonance Raman spectrum of *Rhodobacter sphaeroides* DMSO reductase. These results on LMoO(S-S) complexes are interpreted in the context of the mechanism of sulfite oxidase, the modulation of reduction potentials by a coordinated ene-dithiolate (dithiolene), and the orbital pathway for electron transfer regeneration of pyranopterin dithiolate Mo enzyme active sites.

Introduction

The pterin-containing molybdenum enzymes catalyze a variety of two-electron redox reactions coupled to formal oxygen atom transfer[1−10] but, unlike monooxygenases, the oxygen atom involved in catalysis derives from water instead of dioxygen. X-ray crystallography has begun to define the salient structural features of these enzyme active sites, with the structures of xanthine oxidase related aldehyde oxidoreductase from *Desulfovibrio gigas*,[11,12] the dimethyl sulfoxide (DMSO) reductases from *Rhodobacter capsulatus*[13,14] and *Rhodobacter sphaeroides*,[15] and chicken liver sulfite oxidase[16] all having been recently determined. These studies have revealed that the active sites generally possess at least one Mo≡O unit in the oxidized Mo(VI) state, and all appear to contain at least a single pyranopterin[17] (Figure 1) which is coordinated to Mo via an ene-dithiolate (dithiolene) linkage. Although controversy still exists with respect to whether the crystallographically determined structures reveal the catalytically competent enzyme active site

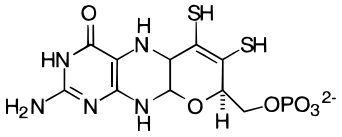

Figure 1. Structure of the pyranopterin derived from protein crystallographic studies (shown in protonated form).[10−16]

[†] The University of New Mexico.
[‡] The University of Arizona.

(1) Hille, R. *Chem. Rev.* **1996**, *96*, 2757−2816.
(2) Young, C. G.; Wedd, A. G. *J. Chem. Soc., Chem. Commun.* **1997**, 1251−1297.
(3) Stiefel, E. I. *J. Chem. Soc., Dalton Trans.* **1997**, 3915−3923.
(4) Enemark, J. H.; Young, C. G. *Adv. Inorg. Chem.* **1993**, *40*, 1−88.
(5) Pilato, R. S.; Stiefel, E. I. In *Bioinorganic Catalysis*; Reedijik, J., Ed.; Dekker: New York, 1993; pp 131−188.
(6) Holm, R. H. *Coord. Chem. Rev.* **1990**, *100*, 183−221.
(7) Rajagopalan, K. V. *Adv. Enzym. Relat. Areas Mol. Biol.* **1991**, *64*, 215−290.
(8) Bastian, N. R.; Kay, C. J.; Barber, M. J.; Rajagopalan, K. V. *J. Biol. Chem.* **1991**, *266*, 45−51.
(9) Johnson, J. L.; Bastian, N. R.; Rajagopalan, K. V. *Proc. Natl. Acad. Sci. U.S.A.* **1990**, *87*, 3190−3194.
(10) Boyington, V. C.; Gladyshev, V. N.; Khangulov, S. V.; Stadtman, T. C.; Sun, P. D. *Science* **1997**, *275*, 1305−1308.
(11) Romão, M. J.; Archer, M.; Moura, I.; Moura, J. J. G.; LeGall, J.; Engh, R.; Schneider, M.; Hof, P.; Huber, R. *Science* **1995**, *270*, 1170−1176.
(12) Huber, R.; Hof, P.; Duarte, R. O.; Moura, J. J. G.; Moura, I.; Liu, M.; LeGall, J.; Hille, R.; Archer, M.; Romão, M. J. *Proc. Natl. Acad. Sci. USA* **1996**, *93*, 8846−8851.
(13) Schneider, F.; Löwe, J.; Huber, R.; Schindelin, H.; Kisker, C.; Knäblein, J. *J. Mol. Biol.* **1996**, *263*, 53−69.
(14) McAlpine, A. S.; McEwan, A. G.; Shaw, A. L.; Bailey, S.*J. Biol. Inorg. Chem.* **1997**, *2*, 690−701.
(15) Schindelin, H.; Kisker, C.; Hilton, J.; Rajagopalan, K. V.; Rees, D. C. *Science* **1996**, *272*, 1615−1621.
(16) Kisker, C.; Schindelin, H.; Pacheco, A.; Wehbi, W. A.; Garrett, R. M.; Rajagopalan, K. V.; Enemark, J. H.; Rees, D. C. *Cell* **1997**, *91*, 973−983.
(17) The generic term "pyranopterin" has been proposed by R. Hille (*JBIC, J. Biol. Inorg. Chem.* **1997**, *2*, 804−809) for the tricyclic heterocycle of Figure 1. For a more detailed discussion of the nomenclature of this tricyclic system and its derivatives, see: Fischer, B.; Enemark, J. H.; Basu, P. *J. Inorg. Biochem.* **1998**, *72*, 13−21.

10.1021/ic981126o CCC: $18.00 © 1999 American Chemical Society
Published on Web 03/19/1999

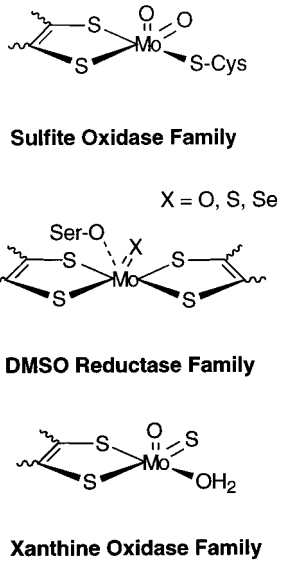

Figure 2. Consensus active site structures for the oxidized Mo(VI) state of the three families of pyranopterin Mo enzymes according to Hille[1]; DMSO reductase family; xanthine oxidase family; sulfite oxidase family.

coordination geometry, the X-ray studies have provided profound insight toward the development of *consensus* structures which correlate the crystallographic results with available EXAFS[18−21] and spectroscopic data. This has allowed for categorizing these Mo enzymes into three main families on the basis of the geometric structure of the oxidized active sites (Figure 2).[1,7]

The crystallographic studies have concluded that the pyranopterin adopts a distinctly nonplanar conformation with an approximately 40° twist of the pyran ring,[10−16,22] strongly favoring a reduced pyranopterin which lacks extensive π-delocalization over the tricyclic ring. Although the pyranopterin is well known to anchor the pyranopterin to the protein via extensive hydrogen bonding,[10−16,22] its precise functional role in catalysis remains undetermined. The intimate association of the pyranopterin dithiolate with Mo suggests a variety of roles for the pyranopterin in catalysis, including modulating the reduction potential and acting as an electron transfer pathway to other endogenous or exogenous redox partners.[1,7] There is structural and reactivity evidence for the direct involvement of the pyranopterin in electron transfer. The structure of *D. gigas* aldehyde oxidoreductase has the amino group of the pterin hydrogen bonded to a cysteinyl sulfur of a 2Fe2S cluster.[12] Also, sulfite oxidase is inactivated by ferricyanide oxidation of the pyranopterin to the fully oxidized state.[23] This study conclusively showed that the presence of a fully oxidized pterin compromised the ability of the enzyme to reduce the physiological oxidant (cytochrome *c*) but did not significantly affect the ability of the enzyme to oxidize sulfite. Therefore, it appears that the oxidized pyranopterin severely retards the egress of reducing equivalents to the endogenous *b*-type heme.

Magnetic circular dichroism (MCD) spectroscopy has been utilized in the study of desulfo-inhibited xanthine oxidase,[24] DMSO reductase,[25] and glycerol-inhibited DMSO reductase,[26] and the MCD spectra of the DMSO reductases have been interpreted in the context of out-of-plane S $p_\pi \rightarrow$ Mo charge transfer transitions. Additionally, resonance Raman spectroscopy[27−29] has been used to probe the lowest energy absorption features observed in the Mo(VI) and Mo(IV) oxidation states of the *R. sphaeroides* enzyme and the vibrational spectra display a complicated series of vibrational bands in the low-frequency region between 250−450 cm^{-1} where metal−ligand vibrations are expected to occur. These vibrational bands were shown to be sensitive to ^{34}S isotopic substitution, indicating that the observed modes possess a significant Mo−S stretching contribution, indicative of the S → Mo charge transfer nature of the low-energy absorption features. Curiously, the multitude of low-frequency vibrations found in DMSO reductase are absent in the resonance Raman spectra of human sulfite oxidase and its C207S mutant.[30] Regardless, the observation of S → Mo charge transfer transitions associated with the Mo-ene-dithiolate portion of the active site has provided the impetus for synthetic and electronic structure studies of model compounds which mimic geometric, spectroscopic, and electron transfer aspects of the active site. Most notable among the spectroscopic work has been a seminal MCD and electronic absorption study which determined that S → Mo LMCT transitions dominate the low-energy absorption and MCD spectra of oxomolybdenum ene-1,2-dithiolate model complexes.[31] The results of this study suggested that the oxomolybdenum ene-1,2-dithiolate moiety is a uniquely designed catalytic unit, allowing for Mo≡O bond destabilization and concomitant activation in oxygen atom transfer catalysis as well as providing an electron transfer conduit coupling Mo with the pyranopterin.

X-ray crystallographic and XAS studies have defined the salient structural features for the pyranopterin centers of Mo enzymes. This allows for detailed spectroscopic studies to be initiated on relevant model complexes in order to develop insight into the electronic origin of observed spectroscopic features and their contributions to reactivity. We have employed a combination of electronic absorption, MCD, and resonance Raman spectroscopies to understand the electronic structure of first generation mono-oxo Mo(V) ene-1,2-dithiolate models for enzymes in the sulfite oxidase family. The results of this spectroscopic study are significant with respect to understanding the mechanism and determining the stereochemical location of the catalytically labile oxo group in sulfite oxidase; providing an emerging picture of how Mo redox potentials may be modulated by a coordinated dithiolate; and describing the orbital pathway for electron transfer regeneration of these Mo enzyme active sites.

(18) Cramer, S. P.; Gray, H. B.; Rajagopalan, K. V. *J. Am. Chem. Soc.* **1979**, *101*, 2772−2774.
(19) George, G. N.; Kipke, C. A.; Prince, R. C.; Sunde, R. A.; Enemark, J. H.; Cramer, S. P. *Biochemistry* **1989**, *28*, 5075−5080.
(20) Cramer, S. P.; Wahl, R.; Rajagopalan, K. V. *J. Am. Chem. Soc.* **1981**, *103*, 7721−7727.
(21) George, G. N.; Garrett, R. M.; Prince, R. C.; Rajagopalan, K. V. *J. Am. Chem. Soc.* **1996**, *118*, 8588−8592.
(22) Chan, M. K.; Mukund, S.; Kletzin, A.; Adams, M. W. W.; Rees, D. C. *Science* **1995**, *267*, 1463−1469.
(23) Gardlik, S.; Rajagopalan, K. V. *J. Biol. Chem.* **1991**, *266*, 4889−4895.
(24) Peterson, J.; Godfrey, C.; Thomson, A. J.; George, G. N.; Bray, R. C. *Biochem. J.* **1986**, *233*, 107−110.
(25) Benson, N.; Farrar, J. A.; McEwan, A. G.; Thompson, A. J. *FEBS Lett.* **1992**, *307*, 169−172.
(26) Finnegan, M. G.; Hilton, J.; Rajagopalan, K. V.; Johnson, M. K. *Inorg. Chem.* **1993**, *32*, 2616−2617.
(27) Gruber, S.; Kilpatrick, L.; Bastian, N. R.; Rajagopalan, K. V.; Spiro, T. G. *J. Am. Chem. Soc.* **1990**, *112*, 8179−8180.
(28) Kilpatrick, L.; Rajagopalan, K. V.; Hilton, J.; Bastian, N. R.; Steifel, E. I.; Pilato, R. S.; Spiro, T. G. *Biochemistry* **1995**, *34*, 3032−3039.
(29) Garton, S. D.; Hilton, J.; Oku, H.; Crouse, B. R.; Rajagopalan, K. V.; Johnson, M. K. *J. Am. Chem. Soc.* **1997**, *119*, 12906−12916.
(30) Garton, S. D.; Garrett, R. M.; Rajagopalan, K. V.; Johnson, M. K. *J. Am. Chem. Soc.* **1997**, *119*, 2590−2591.
(31) Carducci, M. D.; Brown, C.; Solomon, E. I.; Enemark, J. H. *J. Am. Chem. Soc.* **1994**, *116*, 11856−11868.

Experimental Section

General. Unless otherwise noted, all reactions were carried out in an inert atmosphere of nitrogen using Schlenk techniques. All solvents were dried by distillation, and deoxygenated prior to use. Purification of solvents was accomplished using the following methodologies: pyridine and triethylamine from potassium hydroxide; toluene from sodium benzophenone. Other solvents were used without further purification. The compounds $LMoOCl_2$,[32] $LMo^{V}O(tdt)$,[32] $LMo^{V}O(bdt)$,[33,34] and $LMo^{V}O(edt)$[32] were prepared as previously described.

Abbreviations. L, hydrotris(3,5-dimethyl-1-pyrazolyl)borate; bdt, 1,2-benzenedithiolate; tdt, 3,4-toluenedithiolate; edt, 1,2-ethanedithiolate; H_2qdt, quinoxaline-2,3-dithiol; qdt, 2,3-dithioquinoxaline).

Preparation of LMoO(qdt). The reagents 2,3-dihydroxyquinoxaline and phosphorus pentasulfide were purchased from Aldrich Chemical Co. Quinoxaline-2,3-dithiol was prepared by a modified version of Morrison.[35,36] To a dry toluene solution of $LMoOCl_2$ (0.5 g, 1.05 mmol) was added a toluene solution containing 0.41 g (2.1 mmol) of H_2qdt and 150 μL (2.1 mmol) of triethylamine, dropwise by cannula at 70 °C. This solution was allowed to react for approximately 5 h, and during this time the color of the solution changed from lime green to dark red. The resulting dark red solution was filtered and concentrated at reduced pressure to give a dark red powder, which was subsequently redissolved in a minimum amount of toluene and chromatographed on silica gel. The compound eluted in a binary mixture of toluene/1,2-dichloroethane (9:1) as a red band. Yield = 15%. Anal. Calcd for $C_{23}H_{26}N_8OS_2BMo$: C, 45.93; H, 4.36. Found: C, 45.04; H, 4.33. IR (KBr, cm^{-1}): ν(Mo=O) 940, ν(B−H) 2551. MS (FAB): *m*/*z* 602.1 (parent ion), 507 (parent − 3,5-dimethylpyrazole), 410 (parent − dithiolate).

Physical Characterization. Elemental analysis was performed at The University of New Mexico using a Perkin-Elmer 2400 CHN elemental analyzer equipped with a P-E AD-6 Autobalance. Mass Spectra were collected at The Nebraska Center for Mass Spectrometry in the Department of Chemistry at the University of Nebraska—Lincoln.

Electronic Absorption Spectroscopy. Mull and solution electronic absorption spectra were collected on a double beam Hitachi U-3501 UV-vis-NIR spectrophotometer capable of scanning a wavelength region between 185 and 3200 nm. All absorption spectra were collected at 2.0 nm resolution in a single-beam configuration. The instrument was calibrated with reference to the 656.10 nm deuterium line. Immediately following acquisition of the sample spectra, background spectra were collected to correct for residual absorption due to the solvent or mulling agent and to correct for light scattering effects. Solution samples were prepared by dissolving the compounds in degassed dichloroethane. The electronic absorption spectra were subsequently collected in 1 cm pathlength Helma quartz cells (black-masked Suprasil II, equipped with a Teflon stopper). Mull samples were prepared by grinding the solid sample into a fine powder before dispersing it into poly(dimethylsiloxane). The prepared mull was subsequently placed between two 1 mm thick Infrasil quartz discs (ESCO) and secured in a custom designed sample holder. A Janis STVP-100 continuous flow cryostat mounted in a custom designed cradle assembly was used for acquisition of the low-temperature (∼5 K) spectra. The sample temperature was continuously monitored with a Lakeshore silicon-diode (PT-470) and regulated by a combination of helium flow and dual heater assemblies. Gaussian resolution of spectral bands and corrections for light scattering were accomplished with KaleidaGraph and programs incorporated within the Hitachi version of the Grams software package.

Magnetic Circular Dichroism Spectroscopy. Low-temperature MCD data were collected on a system consisting of a Jasco J600 CD spectropolarimeter employing Hamamatsu photomultiplier tubes of either S-1 or S-20 response, an Oxford Instruments SM4000-7T superconducting magneto-optical cryostat (0−7 Tesla and 1.4−300 K), and an Oxford Instruments ITC503 temperature controller. The spectrometer was calibrated for CD intensity and wavelength using camphorsulfonic acid and a Nd-doped reference glass sample (Schott Glass). Solid-state MCD spectra were obtained by dispersing finely ground samples in poly(dimethylsiloxane) and compressing the suspension between two 1 mm thick Infrasil quartz discs (ESCO). Depolarization of the incident radiation was checked by comparing the difference in CD intensity of a standard Ni (+)-tartrate solution positioned before and then after the sample. Samples which depolarized the light by <5% were deemed suitable. The MCD spectra in the 250−800 nm range were obtained at 2.0 nm resolution, and data between 400 and 1050 nm were collected at a fixed slit width of 150 μ. All MCD spectra were collected in an applied magnetic field of 7 Tesla.

Vibrational and Resonance Raman Spectroscopy. Infrared spectra were recorded on a BOMEM MB-100 FT-IR spectrometer as pressed KBr disks. The infrared spectra were utilized to monitor the purity of the compounds, as indicated by the absence of the 962 cm^{-1} Mo≡O stretch associated with the $LMoOCl_2$ precursor complex.[32]

Resonance Raman spectra were collected in a 135° backscattering geometry. A Coherent Innova 70-5 (5W) Ar^+ ion laser was the photon source (457.9−528.7 nm, 9 discrete lines) for inducing Raman scattering. The scattered radiation was dispersed onto a liquid N_2 cooled 1″ Spex Spectrum One CCD detector using a Spex 1877E triple grating monochromator equipped with 600, 1200, and 1800 gr/mm holographic gratings at the spectrographic stage. The laser power at the sample was kept between 40 and 100 mW in order to prevent possible photo- and thermal degradation of the sample. Solid samples were prepared as finely ground powders and dispersed in a NaCl(s) matrix with Na_2SO_4 added as an internal standard. These samples were subsequently sealed in an NMR tube and Raman spectra were obtained by spinning the sample in a modified NMR sample holder/spinner. The samples were maintained at ∼140 ± 10 K by the use of a custom designed cold N_2 gas flow system. The sample temperature was periodically monitored with a Lakeshore silicon diode (PT-470) enclosed in a separate NMR tube. The construction of resonance Raman profiles was accomplished by comparing the integrated intensity of a Raman band at a given excitation wavelength relative to that of the 992.4 cm^{-1} band of Na_2SO_4. All data were scan averaged, and any individual data set with vibrational bands compromised by cosmic events was discarded.

Solution Raman spectra were obtained in degassed benzene and spun in a sealed NMR tube at room temperature. Depolarization ratios were obtained by placing a rotatable polarizer before the polarization scrambler and monochromator entrance slit. Relative Raman intensities (perpendicular and parallel to incident radiation) for a given Raman band were measured relative to the 992 cm^{-1} band of benzene.

Ab Initio Calculations. Ab initio calculations were performed using the Gaussian 94 suite of programs.[37] A 6-31G** basis set was employed in calculating the energies and wavefunctions for the model 1,2-ene-dithiolate ($^-SCH=CHS^-$).

Results

Solution Electronic Absorption Spectra. Figure 3 depicts the room temperature electronic absorption spectrum of LMoO(bdt) between 6000 and 35 000 cm^{-1} in dichloroethane. The spectrum is very similar to that previously reported for LMoO(tdt).[31] However, the transitions observed for LMoO(tdt) are generally shifted to slightly lower energies relative to the corresponding bands in LMoO(bdt). The low-energy region of the spectrum consists of three distinct spectral features (bands **1**, **2**, and **4**) below ∼20 000 cm^{-1}. We have found these bands to be characteristic of LMoO(S-S) compounds, where S-S is a dithiolene or dithiolate ligand which forms a five-membered chelate ring with Mo. Band **3** is very weak, and only discernible in the low-temperature MCD spectra (*vide infra*). The transition energies and molar extinction coefficients for four LMoO(S-S)

(32) Cleland, W. E., Jr.; Barnhart, K. M.; Yamanouchi, K.; Collison, D.; Mabbs, F. E.; Ortega, R. B.; Enemark, J. H. *Inorg. Chem.* **1987**, *26*, 1017−1025.
(33) Dhawan, I. K.; Enemark, J. H. *Inorg. Chem.* **1996**, *35*, 4873−4882.
(34) Dhawan, I. K.; Pacheco, A.; Enemark, J. H. *J. Am. Chem. Soc.* **1994**, *116*, 7911−7912.
(35) Morrison, D. C.; Furst, A. *J. Org. Chem.* **1956**, *21*, 470−471.
(36) Helton, M. E.; Kirk, M. L. Submitted for publication.
(37) Gaussian Incorporated, Pittsburgh, PA.

Table 1. Summary of Electronic Absorption Data for LMoO(S-S) Complexes in Dichloroethane

	E_{max}, cm^{-1} (ϵ, M^{-1} cm^{-1})			
	LMoO(bdt)	LMoO(tdt)	LMoO(qdt)[36]	LMoO(edt)
band 1	9 100 (360)	9 100 (490)	11 300 (170)	11 800 (160)
band 2	13 100 (270)	13 000 (270)	13 700 (130)	15 500 (220)
band 4	19 400 (sh,1220)	19 600 (sh,1320)	19 100 (1050)	20 000 (sh, 570)

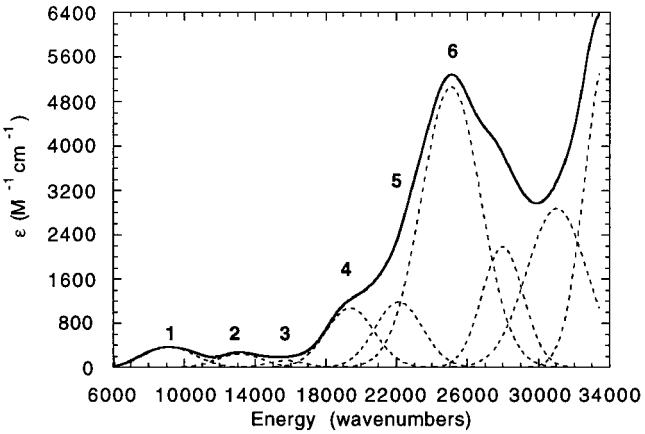

Figure 3. Gaussian-resolved 293 K electronic absorption spectrum of LMoO(bdt) in dichloroethane (2.45×10^{-4} M). The dashed lines represent the individual Gaussians used in the fit.

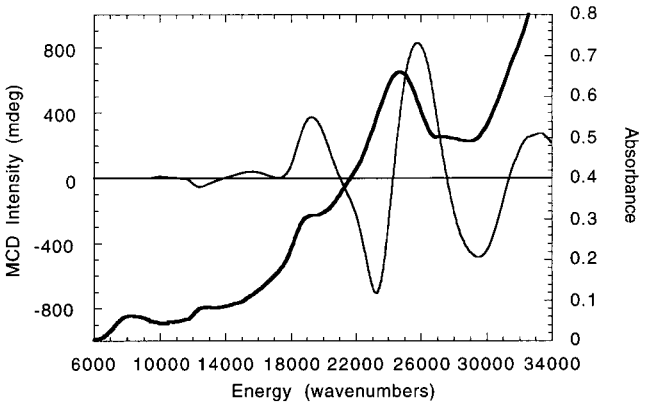

Figure 4. 5 K electronic absorption (heavy line) and 4.86 K MCD (light line) spectra of LMoO(bdt) dispersed in poly(dimethylsiloxane).

complexes are presented in Table 1 for comparative purposes. Of particular interest is band **4**, which is the first absorption feature possessing appreciable intensity characteristic of a charge transfer transition.

Solid-State Electronic Absorption and MCD Spectra. The 5 K mull MCD/absorption overlay of LMoO(bdt) is shown in Figure 4. The electronic absorption spectrum exhibits five distinct features in the solid state with weak to significant intensity. The 21 500 cm^{-1} band is observed as a reproducible shoulder in the mull absorption of LMoO(bdt) but is conspicuously absent in the corresponding absorption spectrum of LMoO(tdt). The general similarity of the solution and mull absorption spectra for LMoO(bdt) indicate that only minor structural changes accompany solvation. This is true for all of the LMoO(S-S) compounds listed in Table 1.

The MCD spectrum of LMoO(bdt) is composed of both C-terms and pseudo A-terms.[38] MCD C-terms possess absorptive bandshapes with intensity maxima at the same energy as corresponding absorption features, while pseudo A-terms possess

(38) Piepho, S. B.; Schatz, P. N. *Group Theory in Spectroscopy with Applications to Magnetic Circular Dichroism*; Wiley-Interscience: New York, 1983.

Table 2. Calculated Oscillator Strengths of LMoO(bdt) and the Relationship between MCD and Electronic Absorption Bands

band no.	$E^{(soln)}_{max}$ (cm^{-1})	oscillator strength	$E^{(mull)}_{max}$ (cm^{-1})	$E^{(MCD)}_{max}$ (cm^{-1})[a]	MCD term[a]
1	9 100	5.6×10^{-3}	8 500	- - - -	- - - -
2	13 100	3.3×10^{-3}	12 700	12 400	−C
3	15 800	- - - -	- - - -	15 700	+C
4	19 400	1.6×10^{-2}	19 200	19 300	+C
5	22 100	1.7×10^{-2}	21 500	21 000	+pseudo A
6	25 100	9.2×10^{-2}	24 600	24 300	+pseudo A

[a] A positive pseudo A-term is a derivative shaped MCD feature with the positive component at higher energy. E_{max} represents the point at which the pseudo A-term changes sign.

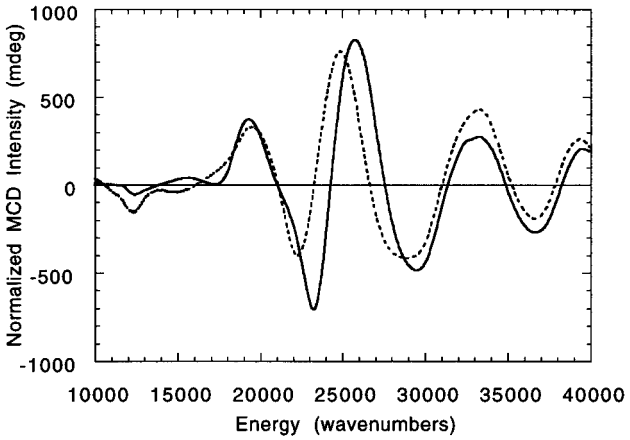

Figure 5. 4.86 K MCD spectra of LMoO(bdt) (solid line) and LMoO(tdt) (dotted line) dispersed in poly(dimethylsiloxane). Note the overall similarity of the spectral features.

derivative-shaped dispersions which possess zero intensity at an energy corresponding to an absorption maximum. The relationship between observed MCD and electronic absorption bands in LMoO(bdt) is given in Table 2.

Figure 5 compares the 5 K/7 T MCD mull spectra of LMoO(bdt) and LMoO(tdt) in the spectral region between 10 000 and 40 000 cm^{-1}. The MCD spectra are seen to be quite similar, and this band pattern is characteristic of LMoO(S-S) complexes where the Mo≡O bond is oriented cis to a single dithiolate ligand which forms a five-membered chelate ring with Mo.[31] However, noticeable differences in MCD sign exist for these compounds in the 14 000−17 000 cm^{-1} range, where no discernible maxima occur in the absorption spectra (see Figure 3). Close inspection of Figure 5 reveals the reason the 21 500 cm^{-1} transition in LMoO(bdt) is not resolved in the MCD or absorption spectra of LMoO(tdt). The positive C-term at 19 300 cm^{-1} and the low-energy negatively signed component of the 24 300 cm^{-1} positive pseudo A-term observed in LMoO(bdt) are energetically compressed in the MCD spectrum of LMoO(tdt), effectively masking the 21 500 cm^{-1} spectral feature. The MCD spectrum of LMoO(qdt) shows this transition as a clearly resolved positive pseudo A-term.[36]

Vibrational Spectra. The IR data for LMoO(bdt) and LMoO(tdt) display intense peaks at 932 and 926 cm^{-1}, respectively. Strong IR bands in the 910−965 cm^{-1} range have been reported for a variety of $LMoOX_2$ complexes,[39−43] and this band has

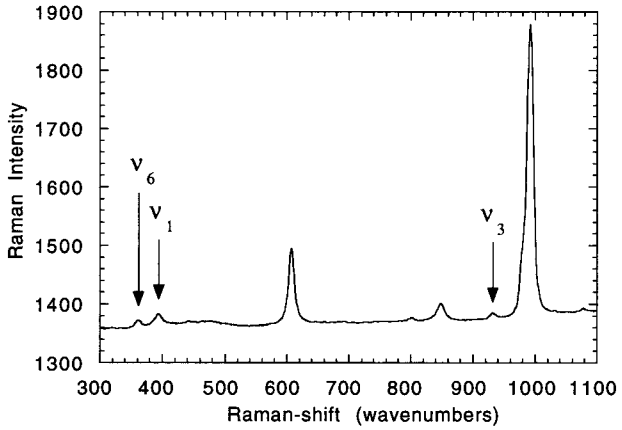

Figure 6. 293 K resonance Raman spectrum of LMoO(bdt) in benzene. The spectrum was obtained with 514.5 nm excitation and the incident laser power at the sample was ~75 mW. Unmarked bands are those of the solvent.

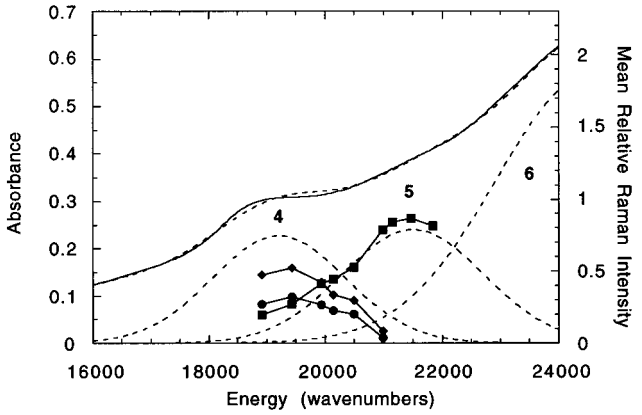

Figure 7. 140 K solid-state resonance Raman excitation profiles for LMoO(bdt). The incident laser power measured at the sample was ~50 mW. The profiles are superimposed on the Gaussian-resolved 5 K mull absorption spectrum of Figure 4. The dashed lines represent the individual Gaussians used in the fit. ν_1 (diamonds), ν_3 (squares), ν_4 (circles).

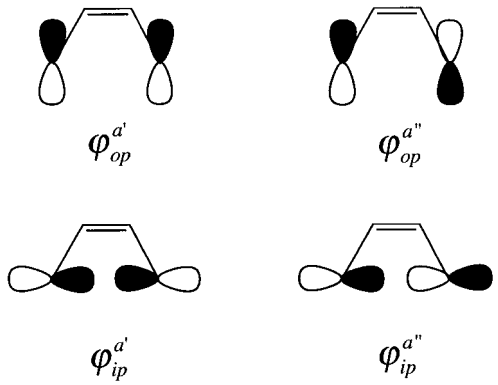

Figure 8. Highest occupied molecular orbitals of the model 1,2-ene-dithiolate, $^{-}$SCH=CHS^{-}. The small amplitudes of the wavefunction on the dithiolate carbon atoms are not shown for clarity.

been assigned as the Mo≡O stretching vibration. Vibrational studies on related compounds possessing the $\{Mo^{V}\equiv O\}^{3+}$ unit also reveal the presence of a band in this region assignable as the Mo≡O stretch.[44−47] The IR spectra are also useful for detecting very small quantities of $LMoOCl_2$ precursor complex that may be present in the sample as a contaminant. No 961 cm^{-1} Mo≡O stretch characteristic of $LMoOCl_2$ was observed in the IR spectra of the LMoO(S-S) complexes used in this study.[32]

Figure 6 shows the 514.5 nm Raman spectrum of LMoO(bdt) in benzene. The solution spectrum contains only three observable vibrational modes between 250 and 1000 cm^{-1}, with frequencies of 362, 393, and 932 cm^{-1}. Vibrational bands in the 300−400 cm^{-1} region of transition metal 1,2-ene-dithiolates have been collectively assigned as Mo-S stretching vibrations.[48−50] A qualitative depolarization study was performed on LMoO(bdt) in benzene using 496.5 nm excitation which yielded depolarization ratios of 0.40 (362 cm^{-1}), 0.22 (393 cm^{-1}), and 0.01(932 cm^{-1}). Since the symmetry of the LMoO(S-S) complexes is very close to C_s, the depolarization ratios for these bands are characteristic of totally symmetric a′ modes. Raman spectra for LMoO(bdt) and LMoO(tdt) were also collected in the solid-state at 140 K using laser excitation at wavelengths between 528.7 and 457.9 nm. As was the case in solution, three vibrational bands were observed. These occured at 362, 393, and 931 cm^{-1} for LMoO(bdt) and at 342, 376, and 926 cm^{-1} for LMoO(tdt). Therefore, no significant ground-state vibrational frequency shifts occur between the solid and solution spectra, providing strong evidence that the structural integrity of these complexes is maintained in solution.

Resonance Raman Excitation Profiles. Resonance Raman excitation profiles were collected in the solid state at 140 K using laser excitation wavelengths between 457.9 and 528.7 nm. This wavelength range encompasses the absorption envelopes of bands **4** and **5**. All three observed vibrational bands for LMoO(bdt) were found to be resonantly enhanced, and the resonance Raman profiles have been superimposed upon the Gaussian resolved 5 K mull absorption spectrum in Figure 7. Extremely *selective* resonance Raman enhancement patterns are evident for excitation into band **4** (362 and 393 cm^{-1} modes) and band **5** (931 cm^{-1} mode). Interestingly, the resonance Raman profile for the corresponding 926 cm^{-1} mode of LMoO(tdt) shows no high-energy turnover when pumping into band **5**. This is consistent with the low-temperature mull absorption and MCD spectra of LMoO(tdt), which indicate that band **6** is lowered in energy and overlaps band **5**. The result implies that the 931 cm^{-1} mode of LMoO(bdt) is also resonantly enhanced when pumping into band **6**.

Ab Initio Calculations. Ab initio calculations on the model ethenedithiolate ($^{-}$SCH=CHS^{-}) fragment resulted in an isolated set of four filled dithiolate orbitals that are primarily sulfur in character, and these are depicted in Figure 8. These are the ligand wavefunctions which can energetically mix and form symmetry-adapted linear combinations (SALC's) with the d orbitals of appropriate symmetry localized on Mo. The calcula-

(39) Chang, C. S. J.; Collison, D.; Mabbs, F. E.; Enemark, J. H. *Inorg. Chem.* **1990**, *29*, 2261−2267.
(40) Chang, C. S. J.; Enemark, J. H. *Inorg. Chem.* **1991**, *30*, 683−688.
(41) Nipales, N.; Westmoreland, T. D. *Inorg. Chem.* **1995**, *34*, 3374−3377.
(42) Lincoln, S. E.; Loehr, T. M. *Inorg. Chem.* **1990**, *29*, 1907−1915.
(43) Chang, C. S. J.; Pecci, T. J.; Carducci, M. D.; Enemark, J. H. *Inorg. Chem.* **1993**, *32*, 4106−4110.
(44) Bradbury, J. R.; Mackay, M. F.; Wedd, A. G. *Aust. J. Chem.* **1978**, *31*, 2423−2430.
(45) Ellis, S. R.; Collison, D.; Garner, C. D. *J. Chem. Soc. Dalton Trans.* **1989**, 413−417.
(46) Burt, R. J.; Dilworth, J. R.; Leigh, G. J.; Zubieta, J. A. *J. Chem. Soc. Dalton Trans.* **1982**, 2295−2298.
(47) Ueyama, N.; Okamura, T.; Nakamura, A. *J. Am. Chem. Soc.* **1992**, *114*, 8129−8137.
(48) Spiro, T. (Ed.) *Molybdenum Enzymes*; John Wiley and Sons: New York, 1985.
(49) Subramanian, P.; Burgmayer, S.; Richards, S.; Szalai, V.; Spiro, T. G. *Inorg. Chem.* **1990**, *29*, 3849−3853.
(50) Oku, H.; Ueyama, N.; Nakamura, A. *Inorg. Chem.* **1995**, *34*, 3667−3676.

tions indicate that the electron density is largely localized on the sulfur atoms, in agreement with experimental results from photoelectron spectroscopy.[51] The four orbitals may be divided into two sets with respect to their orientation to the plane containing the constituent atoms of the ene-dithiolate. These are the in-plane components, $\varphi_{ip}^{a'}$ and $\varphi_{ip}^{a''}$, and the out-of-plane components $\varphi_{op}^{a'}$ and $\varphi_{op}^{a''}$. The superscripts a′ and a″ refer to the symmetry of the wavefunction with respect to the C_s mirror plane. This mirror plane is oriented perpendicular to the ene-dithiolate plane, bisecting the C═C bond.

Analysis

Origin of the S → Mo Charge Transfer. The LMoO(S-S) compounds in Table 1 possess nearly perfect C_s symmetry with respect to the donor atoms which comprise the first coordination sphere. However, an argument can be made that effective C_{4v} symmetry may be utilized due to the presence of the strong field terminal oxo ligand. This is apparent in the nearly axial **A** tensors determined from single-crystal EPR studies on $LMoOCl_2$[52] and EPR simulations of LMoO(bdt)[33,34] and LMoO(edt)[32] frozen solution spectra. From a ligand-field perspective, this would imply nearly degenerate $d_{xz,yz}$ orbitals in the ground state. Recognizing this fact we will utilize $C_{4v} \rightarrow C_{2v} \rightarrow C_s$ descent in symmetry in the analysis of the LMoO(S-S) compounds, keeping in mind the strong axial nature of the ligand field and the anticipated small anisotropy within the equatorial plane.

The oscillator strength of an electronic absorption band is proportional to $|\langle\psi_G|\mathbf{r}|\psi_E\rangle|^2$, where ψ_G and ψ_E are the ground and excited state wavefunctions, and **r** is the position vector.[53−55] In a one-electron approximation, $|\langle\psi_G|\mathbf{r}|\psi_E\rangle|^2 = |\langle\psi_a|\mathbf{r}|\psi_b\rangle|^2$, where ψ_a and ψ_b are the two molecular orbitals involved in the one electron promotion $\psi_a \rightarrow \psi_b$. Metal−ligand covalency results in molecular orbital wavefunctions that can be expanded in terms of metal- and ligand-centered functions:

$$\psi_a = C_1\varphi_M + C_2\varphi_L + ...$$

$$\psi_b = C_1'\varphi_M + C_2'\varphi_L + ...$$

$$\text{where } \varphi_L = \sum_n C_n\chi_n$$

Here, the C_i are the coefficients of the metal (φ_M) and ligand (φ_L) orbitals which constitute the ψ_a and ψ_b ground state molecular orbital wavefunctions. Considering the LMoO(S-S) compounds in this study, φ_M are the Mo d orbitals (e.g., $\varphi_{xy}^{a'}$ etc.); φ_L are the four orthogonal ene-dithiolate orbitals ($\varphi_{ip}^{a'}$, $\varphi_{op}^{a'}$, $\varphi_{ip}^{a''}$, and $\varphi_{op}^{a''}$) of Figure 8, to which the primary contributors are the χ_n for the atomic sulfur p orbital functions. It has been shown that the dominant contributor to the oscillator strengths of all transitions are integrals of the form $\langle\chi_n|\mathbf{r}|\chi_n'\rangle$.[53−55] In the limit of no overlap between the two sulfur p orbitals on different atoms, $\langle\chi_n|\mathbf{r}|\chi_n'\rangle$ reduces to[53]

$$\sum_n C_n C_n' \mathbf{r}\langle\chi_n|\chi_n'\rangle$$

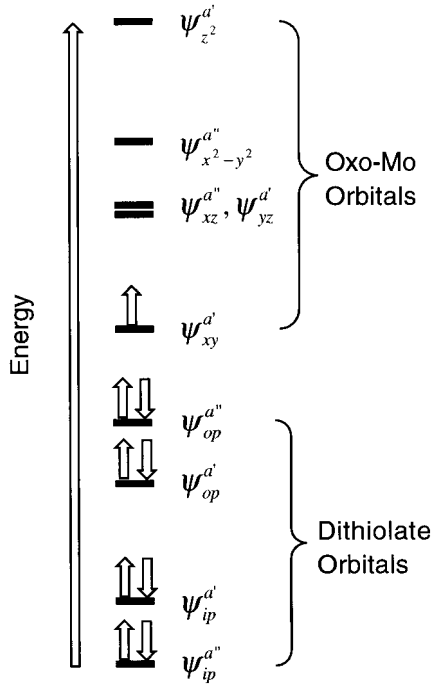

Figure 9. Spectroscopically effective molecular orbital diagram for the LMoO(S-S) complexes. The molecular orbital energies are not to scale. The $\psi_{xz,yz}$ orbitals are shown as degenerate due to the dominance of the strongly bound oxo ligand on the *z* axis.

where C_n and C_n' are the sulfur atomic orbital coefficients in ψ_a and ψ_b, and $\langle\chi_n|\chi_n'\rangle$ is an overlap integral. Thus, the same type of dithiolate molecular orbital (e.g., $\langle\varphi_{ip}|\varphi_{ip}\rangle$ or $\langle\varphi_{op}|\varphi_{op}\rangle$) must be present in the ground and excited wavefunctions for enhanced charge transfer transition intensity, and this intensity is a direct consequence of the Mo d−dithiolate S covalency.

The ligand field splitting of the d-orbital manifold in LMoO(S-S) and other high-valent metal oxo compounds is dominated by the presence of a short 1.7−1.9 Å M≡O bond.[56−59] The terminal oxo ligand is an extremely strong σ- and π-donor, and in the presence of a moderate to weak equatorial ligand field the d-orbital splitting diagram in Figure 9 results. Here, the Mo $\psi_{z^2}^{a'}$ and $\psi_{xz,yz}^{a'',a'}$ orbitals are strongly destabilized by σ and π antibonding interactions with the terminal oxo ligand. In d^1 LMoO(S-S) complexes, all of the d orbitals may act as acceptor orbitals in low-energy LMCT interactions involving the coordinated dithiolate. Therefore, the energy of these charge transfer transitions will be strongly affected by the oxo-mediated destabilization of these acceptor orbitals. Figure 9 also depicts the anticipated relative energy of the lowest ligand field and charge-transfer excitations. As a result of the Mo d orbital splitting pattern, the predicted lowest energy charge transfer transitions will be to the Mo $\psi_{xy}^{a'}$ orbital followed by transitions to the $\psi_{xz,yz}^{a'',a'}$ orbital set. These LMCT transitions originate from the four dithiolate based φ_L molecular orbitals of Figure 8, two of which are oriented within the dithiolate plane ($\varphi_{ip}^{a'}$ and $\varphi_{ip}^{a''}$) and two which are orthogonal to it ($\varphi_{op}^{a'}$ and $\varphi_{op}^{a''}$). It can be seen from this diagram that the stabilization of these dithiolate molecular orbitals will result from specific Mo d−dithiolate S bonding interactions.

(51) Gleiter, R.; Spanget-Larsen, J. *Top. Curr. Chem.: Spectrosc.* **1979**, *86*, 139−196.
(52) Collison, D.; Eardley, D. R.; Mabbs, F. E.; Rigby, K.; Bruck, M. A.; Enemark, J. H.; Wexler, P. A. *J. Chem. Soc. Dalton Trans.* **1994**, 1003−1011.
(53) Avoird, A.; Ros, P. *Theoret. Chim. Acta (Berlin)* **1966**, *4*, 13−21.
(54) Solomon, E. I. *Comm. Inorg. Chem.* **1984**, *3*, 227−320.
(55) LaCroix, L. B.; Shadle, S. E.; Wang, Y.; Averill, B. A.; Hedman, B.; Hodgson, K. O.; Solomon, E. I. *J. Am. Chem. Soc.* **1996**, *118*, 7755−7768.
(56) Ballhausen, C. J.; Gray, H. B. *Inorg. Chem.* **1962**, *1*, 111−122.
(57) Gray, H. B.; Hare, C. R. *Inorg. Chem.* **1962**, *1*, 363−368.
(58) Collison, D. *J. Chem. Soc. Dalton Trans.* **1990**, 2999−3006.
(59) Winkler, J. R.; Gray, H. B. *Comments Inorg. Chem.* **1981**, *1*, 257−263.

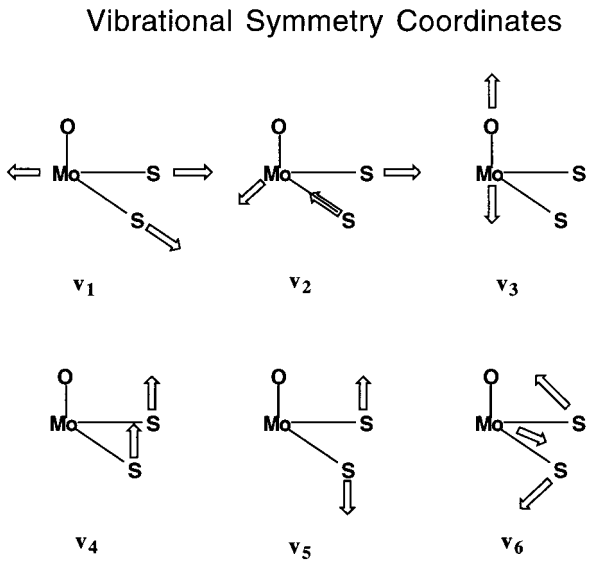

Figure 10. The six vibrational symmetry coordinates for a simple four atom model of the LMoO(S-S) complexes. The true normal modes will be a linear combination of symmetry coordinates possessing the same symmetry.

Gaussian Resolution of the Absorption Spectra. A combination of electronic absorption and MCD spectroscopy has been utilized in order to quantitate the number of distinct electronic transitions below ~28 000 cm^{-1}. A key feature to be recognized is the similarity in energy and intensity of the three lowest energy absorption features for the LMoO(S-S) compounds listed in Table 1. This is strongly indicative of a common electronic origin for each of the three electronic transitions. The low energy transitions (bands **1**, **2**, and **4**) observed in the low-temperature electronic absorption spectra correspond with MCD C-terms. As a result, the solution absorption spectra in this region were fitted with three individual Gaussians. Interestingly, the MCD in the 14 000−17 000 cm^{-1} range (band **3**) is quite complex. This region is dominated by positive MCD intensity in LMoO(bdt) and negative intensity in LMoO(tdt). The absorption intensity here is very weak, and no discernible band maximum is observed. Therefore, band **3** was fit with a single small Gaussian. The two MCD pseudo A-terms (bands **5** and **6**) have been approximated as single unresolved Gaussians in the solution absorption spectra. These MCD pseudo A-terms necessarily derive from $^2B_2 \rightarrow {}^2E$ transitions in C_{4v} ($^2A' \rightarrow {}^2A',{}^2A''$ in C_s). The small low-symmetry splitting of these ^2E states support the results of single-crystal EPR studies on $LMoOCl_2$,[52] which have shown that C_{4v} to C_s symmetry lowering does not have a dramatic effect on the energy splitting of the Mo $d_{xz,yz}$ orbital set. The Gaussian resolution of the LMoO(bdt) solution absorption spectrum was presented in Figure 3, and the results were summarized in Table 2.

Resonance Raman Probes of the S → Mo Charge Transfer. Resonance Raman spectroscopy can be used to directly probe the origin of charge-transfer transitions through the construction of resonance Raman excitation profiles. The spectroscopic innocence of the hydrotris(3,5-dimethyl-1-pyrazolyl)borate ligand results in all LMCT transitions below ~28 000 cm^{-1} being S → Mo in origin.[31] This allows us to focus on a simple, effective four atom MoO(S,S) chromophore. This four atom vibrational model yields the $3N - 6 = 6$ symmetry coordinates listed in Figure 10, which form a basis for the six normal modes of vibration. In this model, S → Mo charge transfer transitions result in excited-state distortions along Mo≡O and Mo−S bonds, and it is these excited state distortions which form the basis for A-term resonance Raman enhancement of totally symmetric normal modes.[60]

Only three vibrations were observed in the solid-state Raman spectra of LMoO(bdt) (362.0, 393.0, and 931.0 cm^{-1}) and LMoO(tdt) (342.0, 376.0, and 926.0 cm^{-1}), and all are resonantly enhanced. The solution Raman depolarization results for LMoO(bdt) show that all three of these vibrations are polarized, providing strong evidence for assigning the vibrational bands as totally symmetric a′ modes. Inspection of Figure 10 reveals that four of the six modes predicted for a C_s MoO(S,S) chromophore are of a′ symmetry. The high-frequency ν_3 mode is easily assigned as the totally symmetric Mo≡O stretch on the basis of its depolarization ratio ($\rho_\parallel/\rho_\perp = 0.01$), high-frequency, strong IR absorption, and analogy to similar oxomolybdenum compounds. There are two vibrational bands found in the 300−400 cm^{-1} region, where Mo−S stretching vibrations are anticipated to occur.[48−50] Since there exists only one totally symmetric a′ S−Mo−S stretch, we assign the 393 cm^{-1} mode as the S−Mo−S stretch (ν_2) and the 362 cm^{-1} as the symmetric S−Mo−S bend (ν_6). The ν_6 bending mode is anticipated to occur at much higher frequency in LMoO(bdt) than in $LMoOCl_2$, since free S···S movement is impeded by the presence of the dithiolate chelate ring. We anticipate a high degree of mode mixing between ν_6 and ν_1 due to their close energy spacing ($\Delta\nu = 31$ cm^{-1}) and the fact that both modes possess a′ symmetry. We have not been able to observe the low frequency a′ dithiolate bend (ν_4). This is probably due to poor resonant enhancement as a result of a very small excited state displacement along this normal coordinate.

There is a marked difference in the LMoO(bdt) resonance Raman enhancement patterns for in-plane (ν_6 and ν_1) and out-of-plane (ν_3) modes. The two in-plane modes, ν_6 and ν_1, are resonantly enhanced within the envelope of band **4**, while ν_3 is resonantly enhanced within the envelope of band **5**. When these profiles are superimposed on the Gaussian-resolved mull absorption spectrum in Figure 7, it becomes clear that the electronic origins of bands **4** and **5** are radically different from one another. These remarkably orthogonal resonance Raman enhancement patterns are indicative of LMCT transitions strongly localized in the dithiolate−Mo plane (band **4**) and perpendicular to it along the Mo≡O bond (band **5**). The resonance enhancement of ν_6 and ν_1 provide direct evidence for band **4** being an in-plane LMCT transition. This is the first direct evidence for the involvement of the $\varphi_{ip}^{a'}$ dithiolate orbital in the low-energy charge transfer spectra of biomimetic oxomolybdenum/oxotungsten dithiolate compounds. Finally, the presence of the obscured band **5** has been definitively confirmed by the ν_3 profile. This is significant, since it is a new band not observed in the MCD or absorption spectra of LMoO(tdt) due to overlapping transitions.

Band Assignments. A combination of descent in symmetry ($C_{4v} \rightarrow C_{2v} \rightarrow C_s$) and orbital overlap considerations have been utilized in order to assign bands **1**−**6**. The inherently low oscillator strengths of the Mo ligand field bands in oxomolybdenum complexes[61,62] ($\epsilon < 100$ M^{-1} cm^{-1}), coupled with the presence of low-energy LMCT excitations, render these transitions difficult to observe in LMoO(S-S) compounds. As a result, LMCT bands are anticipated to dominate the absorption spectra.

Bands 1 and 2. These are the two lowest energy absorption

(60) Albrecht, A. C. *J. Chem. Phys.* **1961**, *34*, 1476−1484.
(61) Garner, C. D.; Lambert, P.; Mabbs, F. E.; King, T. J. *J. Chem. Soc. Dalton Trans.* **1977**, 1191−1198.
(62) Pence, H. E.; Selbin, J. *Inorg. Chem.* **1969**, *8*, 353−358.

features observed in all four of the LMoO(S-S) compounds listed in Table 1. Band **1** is too low in energy to be assigned as the $\psi_{xy}^{a'} \rightarrow \psi_{xz}^{a''},\psi_{yz}^{a'}$ LF transition, and thus it is assigned as a LMCT transition. The oscillator strengths for these two low energy transitions are relatively low ($\epsilon \sim 133-449$ M^{-1} cm^{-1}), allowing for their assignment as $\psi_{op}^{a''} \rightarrow \psi_{xy}^{a'}$ or $\psi_{op}^{a'} \rightarrow \psi_{xy}^{a'}$. Band **1** corresponds to an single MCD C-term which is positive for LMoO(tdt),[31] LMoO(edt),[31] and LMoO(qdt).[36] However, the sign of the MCD C-term is variable for band **2**, being positive for LMoO(edt) and negative for LMoO(bdt), LMoO(tdt), and LMoO(qdt). Since the sign of the C-term for these transitions is governed by spin-orbit coupling with other excited states,[38] the variation for band **2** most reasonably results from differences in out-of-state spin−orbit coupling among the four LMoO(S-S) complexes of Table 1. The definitive energy ordering of the $\psi_{op}^{a''} \rightarrow \psi_{xy}^{a'}$ and $\psi_{op}^{a'} \rightarrow \psi_{xy}^{a'}$ transitions is unknown and requires the explicit evaluation of out-of-state spin-orbit coupling matrix elements. In summary, these $\psi_{op} \rightarrow \psi_{xy}$ transitions are anticipated to occur at low energy and possess relatively low absorption intensity due to poor orbital overlap.

Band 3. This band is assigned as the $\psi_{xy}^{a'} \rightarrow \psi_{xz}^{a''},\psi_{yz}^{a'}$ LF band, which has been observed in the 13 000−16 000 cm^{-1} region for a variety of oxomolybdenum(V) compounds.[63] For example, this transition occurs at 16 000 cm^{-1} ($\epsilon = 17$ M^{-1} cm^{-1}) in $[MoOCl_4]^-$ (C_{4v} symmetry) and at 14 180 cm^{-1} ($\epsilon = 50$ M^{-1} cm^{-1}) for $LMoOCl_2$ (C_s symmetry).[31] The transition is very weak, displaying no discernible absorption feature that corresponds with the positive C-term in the MCD spectrum of LMoO(bdt), and the negative C-term for LMoO(tdt) and LMoO(qdt). No MCD C-term was observed in this region for LMoO(edt), presumably due to a combination of weak intensity and masking by the more intense band **4**. The $\psi_{xy}^{a'} \rightarrow \psi_{xz}^{a''},\psi_{yz}^{a'}$ transition should manifest itself as a pseudo A-term in the MCD spectrum, but this is not observed experimentally. Again, this is most likely due to complications arising from low, inequivalent oscillator strengths for the individual $\psi_{xy}^{a'} \rightarrow \psi_{xz}^{a''}$ and $\psi_{xy}^{a'} \rightarrow \psi_{yz}^{a'}$ components coupled with out-of-state spin-orbit coupling.

Band 4. This is the first intense ($\epsilon = 1220$ M^{-1} cm^{-1} for LMoO(bdt)) LMCT transition in the LMoO(S-S) complexes and is assigned as the in-plane $\psi_{ip}^{a'} \rightarrow \psi_{xy}^{a'}$ LMCT transition based on the resonance Raman enhancement of both ν_6 and ν_1 in-plane vibrational modes within the envelope of this band in LMoO(bdt). The intensity of this band directly probes the degree of $\varphi_{xy}^{a'}-\varphi_{ip}^{a'}$ orbital mixing since it is a bonding → antibonding transition.

The $\psi_{xy}^{a'} \rightarrow \psi_{x^2-y^2}^{a''}$ ligand field transition is also anticipated to occur in this region. Where this transition has been clearly observed as an *isolated* band, the intensity has been found to be very low.[61,62] This is partially due to the fact that this transition is orbitally forbidden in the parent C_{4v} symmetry[31] ($\epsilon = 9$ M^{-1} cm^{-1} for $[MoOCl_4]^-$), as well as being forbidden in C_{2v} symmetry. The effects of symmetry lowering can be found in $[MoOCl_3\{P(NMe_2)_3O\}_2]$, which possesses C_s symmetry with three Cl^- ligands in the equatorial plane.[61] The extinction coefficient of the $\psi_{xy}^{a'} \rightarrow \psi_{x^2-y^2}^{a''}$ transition for this compound is only 20 M^{-1} cm^{-1}. Therefore, intensity enhancement of $\psi_{xy}^{a'} \rightarrow \psi_{x^2-y^2}^{a''}$ due to symmetry lowering appears to be minor. Only the $\psi_{ip}^{a'} \rightarrow \psi_{x^2-y^2}^{a''}$ and $\psi_{op}^{a'} \rightarrow \psi_{x^2-y^2}^{a''}$ LMCT excited states can configurationally mix with $\psi_{xy}^{a'} \rightarrow \psi_{x^2-y^2}^{a''}$ to provide an intensity borrowing mechanism for enhanced oscillator strength of the ligand field band. However, the $\psi_{op}^{a'} \rightarrow \psi_{x^2-y^2}^{a''}$ transition is not anticipated to provide an efficient intensity gaining mechanism for the $\psi_{xy}^{a'} \rightarrow \psi_{x^2-y^2}^{a''}$ LF transition since it is an $\psi_{op} \rightarrow \psi_{ip}$ transition and is predicted to possess low intensity (see bands **1** and **2**). Furthermore, intensity borrowing is expected to be minimal due to the high energy of the $\psi_{op}^{a'} \rightarrow \psi_{x^2-y^2}^{a''}$ and $\psi_{ip}^{a'} \rightarrow \psi_{x^2-y^2}^{a''}$ states, which are predicted to occur at energies greater than 30 000 and 40 000 cm^{-1}, respectively. As a result, the $\psi_{xy}^{a'} \rightarrow \psi_{x^2-y^2}^{a''}$ LF transition is most likely buried under the envelope of the intense $\psi_{ip}^{a'} \rightarrow \psi_{xy}^{a'}$ LMCT transition.

Band 5. The band is assigned as the $\psi_{op}^{a''} \rightarrow \psi_{xz}^{a''},\psi_{yz}^{a'}$ LMCT transition. This is consistent with the resonance Raman enhancement of ν_3, since the $\psi_{op}^{a''} \rightarrow \psi_{xz}^{a''},\psi_{yz}^{a'}$ transition formally results in the promotion of an electron from an out-of-plane dithiolate molecular orbital to a Mo-based orbital which is strongly antibonding with respect to the Mo≡O bond. This transition is observed as a weak shoulder in the low-temperature mull absorption spectrum of LMoO(bdt), and is not discernible in the absorption spectra of LMoO(tdt), LMoO(qdt), or LMoO(edt). Gaussian resolution of the LMoO(bdt) absorption spectrum yields a molar extinction coefficient of ~1100 M^{-1} cm^{-1}. The $\psi_{op}^{a''} \rightarrow \psi_{xz}^{a''},\psi_{yz}^{a'}$ transition is observed as a poorly resolved pseudo A-term feature in the MCD of LMoO(bdt) but is clearly resolved in the LMoO(qdt) spectrum.[36] The pseudo A-term bandshape is a direct manifestation of dominant in-state spin−orbit coupling governing the magnitude of the MCD intensity.

Band 6. This transition is easily assignable as the $\psi_{op}^{a'} \rightarrow \psi_{xz}^{a''},\psi_{yz}^{a'}$ counterpart to band **5**, due to its pseudo A-term character. This transition is higher in energy than $\psi_{op}^{a''} \rightarrow \psi_{xz}^{a''}, \psi_{yz}^{a'}$ since $\psi_{op}^{a'}$ is stabilized relative to $\psi_{op}^{a''}$ by virtue of its interaction with $\psi_{xy}^{a'}$.

In summary, the combination of electronic absorption, MCD, and resonance Raman spectra have been interpreted in the context of ligand field and group theoretical arguments, allowing for a reasonable assignment of the six lowest energy transitions in LMoO(S-S) compounds. However, definitive assignment of the electronic transitions below 18,000 cm^{-1} is difficult due to complications arising from inherently low oscillator strength and out-of-state spin-orbit coupling.

Covalency Contributions to $\psi_{xy}^{a'}$. The electronic structure of these LMoO(S-S) complexes derives from a combination of two factors. The first is the strong axial σ- and π-donor properties of the terminal oxo ligand, which dominates the ligand field and predetermines the energy of the Mo based acceptor orbitals. The second is the equatorial dithiolate sulfur donors, which are the origin of the low energy LMCT features. Dithiolate covalency contributions to $\psi_{xy}^{a'}$ can be directly probed via the relative oscillator strengths of the $\psi_{op}^{a'} \rightarrow \psi_{xy}^{a'}$ and $\psi_{ip}^{a'} \rightarrow \psi_{xy}^{a'}$ transitions. These three wavefunctions may be expanded below in terms of Mo- and dithiolate-based functions:

$$\psi_{xy}^{a'} = c_1\varphi_{xy}^{a'} + c_2\varphi_{ip}^{a'} + c_3\varphi_{op}^{a'}$$

$$\psi_{ip}^{a'} = c_1'\varphi_{xy}^{a'} + c_2'\varphi_{ip}^{a'} + c_3'\varphi_{op}^{a'}$$

$$\psi_{op}^{a'} = c_1''\varphi_{xy}^{a'} + c_2''\varphi_{ip}^{a'} + c_3''\varphi_{op}^{a'}$$

The oscillator strength (f) of the LMoO(S-S) $\psi_{ip}^{a'} \rightarrow \psi_{xy}^{a'}$ LMCT transition is approximately 2.6−6.0 times more intense than the lower energy $\psi_{op}^{a'} \rightarrow \psi_{xy}^{a'}$ transitions. The square root of the oscillator strength for the $\psi_{op}^{a'} \rightarrow \psi_{xy}^{a'}$ transition is proportional to $c_2c_2''\langle\varphi_{ip}^{a'}|\varphi_{ip}^{a'}\rangle + c_3c_3''\langle\varphi_{op}^{a'}|\varphi_{op}^{a'}\rangle$, since $\langle\varphi_{ip}^{a'}|\varphi_{op}^{a'}\rangle = 0$ due to the

(63) Lever, A. B. P. *Inorganic Electronic Spectroscopy*, 2nd ed.; Elsevier Science Publishing: New York, 1986; p 241.

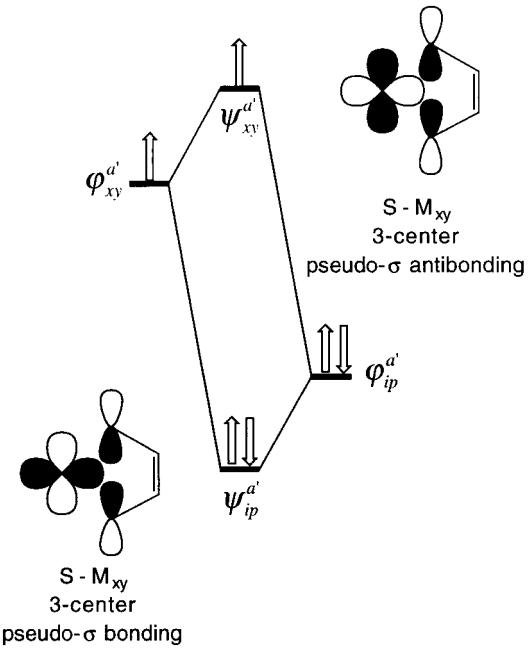

Figure 11. Molecular orbital diagram showing the psuedo-σ bonding and antibonding combinations of the Mo $\varphi_{xy}^{a'}$ and dithiolate $\varphi_{ip}^{a'}$ orbitals.

orthogonality of the S p_z and $p_{x,y}$ atomic orbitals. Similarly, $f^{1/2}$ for the $\psi_{ip}^{a'} \rightarrow \psi_{xy}^{a'}$ transition is proportional to $c_2c_2'\langle\varphi_{ip}^{a'}|\varphi_{ip}^{a'}\rangle + c_3c_3'\langle\varphi_{op}^{a'}|\varphi_{op}^{a'}\rangle$. Clearly, the oscillator strength ratio indicates that $c_2 > c_3$ in the ground state, and covalency contributions to $\psi_{xy}^{a'}$ are dominated by $\varphi_{ip}^{a'}$. If we make the approximation[64] that the oscillator strengths of $\psi_{ip}^{a'} \rightarrow \psi_{xy}^{a'}$ and $\psi_{op}^{a'} \rightarrow \psi_{xy}^{a'}$ are determined solely by the ligand coefficients in $\psi_{xy}^{a'}$, then the c_2^2/c_3^2 ratio is ~2.6−6.0. This seems reasonable and provides an estimate of anisotropic (in-plane vs out-of-plane) covalency contributions to Mo−dithiolate bonding in the ground state $\psi_{xy}^{a'}$ HOMO wavefunction.

Discussion

The results of this study have provided for a reasonable assignment of the low-energy dithiolate → Mo charge transfer transitions, which are the dominant spectral features in LMoO(S-S) compounds. In particular, resonance Raman spectroscopy has been extremely useful in the definitive assignment of the $\psi_{op}^{a''} \rightarrow \psi_{xz}^{a''},\psi_{yz}^{a'}$ and $\psi_{ip}^{a'} \rightarrow \psi_{xy}^{a'}$ LMCT transitions by virtue of their radically different excitation profiles. A significant distortion along the ν_1 and ν_6 Mo−S modes accompanies the $\psi_{ip}^{a'} \rightarrow \psi_{xy}^{a'}$ transition, indicative of a substantial change in in-plane Mo−dithiolate bonding accompanying this one-electron promotion to the Mo−dithiolate antibonding $\psi_{xy}^{a'}$ orbital. The $\psi_{op}^{a''} \rightarrow \psi_{xz}^{a''},\psi_{yz}^{a'}$ transition results in an excited state distortion along ν_3 and a concomitant weakening of the Mo≡O bond. Although resonance Raman enhancement of ν_4 may have been anticipated, it was not observed. Presumably, the distortion along this out-of-plane Mo−S symmetric bending mode is very small.

The definitive assignment of band **4** as $\psi_{ip}^{a'} \rightarrow \psi_{xy}^{a'}$, a bonding-to-antibonding transition is extremely important. Figure 11 depicts the bonding and antibonding combinations between the Mo $\varphi_{xy}^{a'}$ and in-plane S $\varphi_{ip}^{a'}$ orbitals. The Mo $\varphi_{xy}^{a'}$ orbital derives from the t_{2g} set in O_h and is a π-type orbital with respect to bonding interactions with simple monodentate donor ligands. However, the $\varphi_{ip}^{a'}$ orbital of the dithiolate ligand is positioned for good overlap with the Mo $\varphi_{xy}^{a'}$ orbital to give a special three-center pseudo-σ type bonding interaction (Figure 11). The energy of the $\psi_{ip}^{a'} \rightarrow \psi_{xy}^{a'}$ LMCT transition (band **4**) reflects the strength of this bonding interaction, and the intensity of the band directly probes the pseudo-σ mediated Mo−dithiolate covalency.[65]

The energy of $\psi_{xy}^{a'}$ is primarily affected by the nature of the equatorial ligand field, and strong pseudo-σ Mo-dithiolate bonding raises the energy of this orbital. Additionally, the effective nuclear charge (Z'_{eff}) of the metal is a property of the donor atoms, and appreciable changes in Z'_{eff} for Mo may be anticipated as a result of the highly polarizable dithiolate sulfur donor ligands.[66] The relatively high intensity of the $\psi_{op}^{a'} \rightarrow \psi_{xz}^{a''}$, $\psi_{yz}^{a'}$ and $\psi_{op}^{a''} \rightarrow \psi_{xz}^{a''},\psi_{yz}^{a'}$ LMCT transitions in the LMoO(S-S) complexes reflects the π-donor character of the dithiolates and the concomitant reduction in Z'_{eff} due to π-mediated charge donation to Mo. Thus, the relative π-donor properties of the dithiolate ligand can modulate the reduction potential of the Mo center by affecting the valence ionization energy of the $\psi_{xy}^{a'}$ orbital through changes in Z'_{eff} on Mo.

The observed oscillator strength of the $\psi_{ip}^{a'} \rightarrow \psi_{xy}^{a'}$ transition for the LMoO(S-S) compounds depends on the ligand backbone. The intensity of this transition for LMoO(edt), which has a C-C single bond, is a factor of two less than that observed for the other LMoO(S-S) compounds that possess an aromatic dithiolate C−C bond. The large $\psi_{ip}^{a'}-\psi_{xy}^{a'}$ in-plane covalency for ene-dithiolates suggests that this interaction, in concert with π-delocalization, may play a major role in the unusual ability of these ligands to support multiple redox states[67] and to electronically buffer metal centers to large changes in charge.[68] The possible role of in-plane covalency in electron transfer in pterin-containing molybdenum enzymes is discussed below.

Implications for Enzymes. The spectroscopic studies of the LMoO(S-S) compounds discussed above provide a framework for discussing the electronic structures and properties of *cis*-MoO(ene-dithiolate) units in enzymes. The domination of the ligand field by the Mo≡O group isolates $\psi_{xy}^{a'}$ as the redox orbital and restricts its spatial orientation to the plane perpendicular to the Mo≡O vector. The interactions of $\varphi_{xy}^{a'}$ with the $\varphi_{ip}^{a'}$ and $\varphi_{op}^{a'}$ orbitals of an ene-dithiolate oriented cis to Mo≡O are depicted in Figure 12. These bonding interactions further perturb the energy of $\psi_{xy}^{a'}$ and hence the reduction potential of the Mo center. The interactions of Figure 12 also affect the electron density distribution in $\psi_{xy}^{a'}$ and are thereby expected to play a significant role in providing for efficient coupling into protein mediated superexchange pathways.[69] As a result, we have formulated an "oxo-gate" hypothesis whereby a single Mo≡O bond oriented cis to the dithiolate plane is a necessary

(64) The approximation that the oscillator strengths of the $\psi_{ip}^{a'} \rightarrow \psi_{xy}^{a'}$ and $\psi_{op}^{a'} \rightarrow \psi_{xy}^{a'}$ transitions are determined solely by the ligand coefficients in $\psi_{xy}^{a'}$ is supported by density functional calculations on [MoO(ethenedithiolate)$_2$]$^-$. McNaughton, R.; Kirk, M. L. Manuscript in preparation.

(65) The pseudo-σ interaction refers to the three-center bonding interaction that occurs between the Mo based $\varphi_{xy}^{a'}$ orbital and the $\varphi_{ip}^{a'}$ LCAO of the dithiolate chelate.

(66) The exceptionally strong σ and π donor oxo ligand also plays a profound role in modulating Z'_{eff}. Changes in the nature of the pyranopterin-dithiolate may play a greater role in affecting *changes* in Z'_{eff} during the course of catalysis and/or determining differences among the various pyranopterin Mo enzymes.

(67) Burns R. P.; McAuliffe C. A. *Adv. Inorg. Chem.* **1979**, *22*, 303−348.
(68) Westcott, B. L.; Gruhn, N. E.; Enemark, J. H. *J. Am. Chem. Soc.* **1998**, *120*, 3382−3386.
(69) Holm, R.; Kennepohl, P.; Solomon, E. I. *Chem. Rev.* **1996**, *96*, 2239−2314.

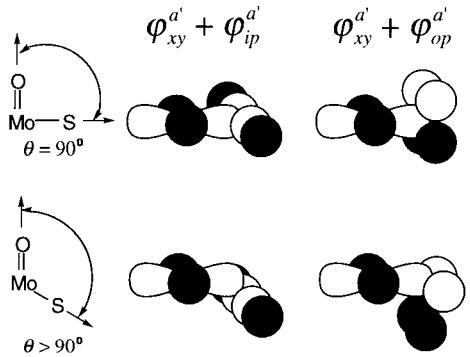

Figure 12. Orbital interaction diagram detailing how the $\varphi_{xy}^{a'}$ orbital mixes with $\varphi_{ip}^{a'}$ and $\varphi_{op}^{a'}$ as a function of the O≡Mo−S angle. The $\varphi_{xy}^{a'}-\varphi_{ip}^{a'}$ interaction is maximized at $\theta = 90°$ and decreases with increasing O≡Mo−S angle. The $\varphi_{xy}^{a'}-\varphi_{op}^{a'}$ overlap is minimized at $\theta = 90°$ and increases as the O≡Mo−S angle increases.

condition for efficient electron transfer regeneration of pyranopterin Mo enzyme active sites following formal oxygen atom transfer.

Facile electron transfer regeneration requires that there be a high degree of electronic communication between donor and acceptor sites. The magnitude of the electron transfer coupling matrix element (H_{DA}), between donor and acceptor sites, is affected by the degree of metal−ligand covalency;[69] anisotropy in this covalency (dictated by the nature of the ligand donor set, σ vs π bonding, in-plane vs out-of-plane bonding contributions); and electron tunneling through the protein matrix.[70,71] Although there has been considerable effort expended in understanding the contributions of electron tunneling through proteins,[70,71] the effects of metal−ligand covalency are in general much less understood, having been studied in detail only for blue copper proteins[72] and rubredoxin.[73] If the pyranopterin-dithiolate is directly involved in an effective electron transfer regeneration pathway, good overlap must exist between the Mo $\varphi_{xy}^{a'}$ orbital and at least one of the dithiolate orbitals of the same symmetry ($\varphi_{ip}^{a'}$ and $\varphi_{op}^{a'}$). In fact, the magnitude of H_{DA} is a function of this overlap and is proportional to the square of the molecular orbital coefficients c_2 and c_3.[74] The spectroscopically determined c_2^2/c_3^2 ratio for LMoO(bdt) is ∼2.6−6.0. Thus, the electron-transfer rate, which is proportional to H_{DA}^2, is anticipated to be approximately 7−36 times more efficient via the pseudo-σ $\varphi_{xy}^{a'}-\varphi_{ip}^{a'}$ pathway than through the $\varphi_{xy}^{a'}-\varphi_{op}^{a'}$ pathway. This is important because the structure of the pyranopterin favored by current evidence (Figure 1) has a reduced (formally tetrahydro) pyrazine ring located between the Mo−dithiolate fragment and the π-system of the pyrimidine ring of the pyranopterin. Thus, the pyranopterin structure of Figure 1 presents a poor π electron transfer pathway; efficient π-mediated electron transfer for a reduced pyranopterin would require scission of the pyran ring to give a specific dihydropterin as well as a more covalent $\varphi_{xy}^{a'}-\varphi_{op}^{a'}$ interaction to couple $\varphi_{xy}^{a'}$ into the π-system.[75] Therefore, we propose that the pathway of pyranopterin mediated electron transfer most likely involves the σ-orbitals.

Efficient electron transfer rates should also be facilitated by minimimal reorganizational energy of the active site. Our resonance Raman profiles conclusively show that one-electron promotions into the monooxo Mo $\psi_{xy}^{a'}$ redox orbital (band **4**) result in no appreciable distortion along the high-frequency Mo≡O stretching mode.

The consensus active site structure of sulfite oxidase derived from X-ray crystallography and EXAFS (Figure 2c) raises the question as to which oxo ligand is directly involved in the catalytic oxidation of sulfite to sulfate. Crystallography has shown that the active site is deeply buried within the Mo binding domain, and that substrate has access only to the oxo ligand residing in the equatorial plane.[16] The equatorial oxo ligand is also anticipated to be the reactive oxo ligand from an electronic structure viewpoint. Formal oxygen atom transfer results in a reduced mono-oxo Mo(IV) site with the apical Mo≡O bond oriented perpendicular to the dithiolate plane, allowing for efficient pyranopterin−dithiolate-mediated electron transfer regeneration of the active site. In the reduced state, a H_2O molecule or OH^- occupies this equatorial site. According to our oxo-gate hypothesis, H_2O/OH^- only becomes fully deprotonated following the transfer of the second electron, resulting in the fully oxidized dioxo Mo(VI) state which is then fully competent for substrate oxidation. The Mo(VI) redox orbital is now no longer oriented in a manner conducive with favorable interactions involving the dithiolate portion of the pyranoterin. This should have the effect of lowering the Mo reduction potential and decoupling the Mo site from the electron transfer pathway, thereby preventing accidental reduction of the active site prior to catalysis.

Summary

Detailed spectroscopic studies on LMoO(S-S) model complexes have been undertaken in order to develop insight into the electronic origin of observed spectroscopic features and relate these to electron transfer and oxo transfer reactivity in the pyranopterin Mo enzymes. The results of this work are significant, detailing a highly covalent interaction between the redox active Mo $\varphi_{xy}^{a'}$ atomic orbital and the dithiolate $\varphi_{ip}^{a'}$ SALC. This is a remarkable three-center pseudo-σ type bonding interaction which couples the $\varphi_{xy}^{a'}$ orbital directly into the in-plane orbitals of the pyranopterin. This effective in-plane covalency is anticipated to play an important role in modulating the reduction potential of the active site by destabilizing $\psi_{xy}^{a'}$. The Mo≡O group controls the orientation of $\varphi_{xy}^{a'}$, and $\varphi_{xy}^{a'}-\varphi_{ip}^{a'}$ overlap is maximized when the dithiolate chelate is oriented cis to the Mo≡O bond. This has resulted in the development of an oxo-gate hypothesis, whereby the Mo reduction potential and the coupling of $\varphi_{xy}^{a'}$ to electron transfer pathways involving the σ system of the pyranopterin are dictated by the orientation of the Mo≡O bond(s) relative to the dithiolate chelate. This oxo-gate hypothesis has important implications for the mechanism of sulfite oxidase, where the catalytically labile oxo ligand resides in the equatorial plane, and the axial oxo ligand appears to be an essential requirement for facile electron transfer to regenerate the active site of the enzyme.

Acknowledgment. The authors thank Prof. Partha Basu for substantive comments. We gratefully acknowledge the generous financial support of the The National Institutes of Health (Grant No. GM-057378 to M.L.K. and Grant No. GM-37773 to J.H.E.).

IC981126O

(70) Beratan, D. N.; Betts, J. N.; Onuchic, J. N. *Science* **1991**, *252*, 1285−1288.
(71) Beratan, D. N.; Onuchic, J. N.; Betts, J. N.; Bowler, B. E.; Gray, H. B. *J. Am. Chem. Soc.* **1990**, *112*, 7915−7921.
(72) Solomon, E. I. Baldwin, M. J.; Lowery, M. D. *Chem. Rev.* **1992**, *92*, 521−542.
(73) Lowery, M. D.; Guckert, J. A.; Gebhard, M. S.; Solomon, E. I. *J. Am. Chem. Soc.* **1993**, *115*, 3012−3013.
(74) Balaji, V.; Ng, L.; Jordan, K. D.; Paddon-Row, M. N.; Patney, H. K. *J. Am. Chem. Soc.* **1987**, *109*, 6957−6969.
(75) Enemark, J. H.; Garner, C. D. *JBIC, J. Biol. Chem.* **1997**, *2*, 817−822.